Geometry Flexibility of Copper Iodide Clusters: Variability in Luminescence Thermochromism.

Quentin Benito, Xavier F Le Goff, Gregory Nocton, Alexandre Fargues, Alain Garcia, Aurélie Berhault, Samia Kahlal, Jean-Yves Saillard, Charlotte Martineau, Julien Trébosc, et al.

HAL Id: hal-01141761

https://hal-univ-rennes1.archives-ouvertes.fr/hal-01141761

Submitted on 13 Apr 2015

Geometry Flexibility of Copper Iodide Clusters: Variability in Luminescence Thermochromism

Quentin Benito,[†] Xavier F. Le Goff,[‡] Gregory Nocton,[‡] Alexandre Fargues,[§] Alain Garcia,[§] Aurélie Berhault,[||,⊥] Samia Kahlal,[||,⊥] Jean-Yves Saillard,[||,⊥] Charlotte Martineau,[#] Julien Trébosc,[⊗,○] Thierry Gacoin,[†] Jean-Pierre Boilot,[†] and Sandrine Perruchas*[,†]

[†]Laboratoire de Physique de la Matière Condensée (PMC) and [‡]Laboratoire de Chimie Moléculaire, CNRS−Ecole Polytechnique, 91128 Palaiseau Cedex, France

[§]Institut de Chimie de la Matière Condensée de Bordeaux (ICMCB), CNRS, 87 Avenue du Docteur A. Schweitzer, 33608 Pessac Cedex, France

[||]UMR-CNRS, 6226 Institut des Sciences Chimiques de Rennes, Université de Rennes 1, 35042 Rennes Cedex, France

[⊥]Université Européenne de Bretagne, 5 bd. Laënnec, 35000 Rennes, France

[#]Tectospin, Institut Lavoisier de Versailles (ILV), UMR CNRS 8180, Université de Versailles St-Quentin en Yvelines (UVSQ), 45, avenue des Etats-Unis, 78035 Versailles Cedex, France

[⊗]Science et Technologies, Université Lille, F-59000 Lille, France

[○]NRS UMR 8181, Unité de Catalyse et de Chimie du Solide−UCCS; ENSCL, F-59652 Villeneuve d'Ascq, France

Ⓢ *Supporting Information*

ABSTRACT: An original copper(I) iodide cluster of novel geometry obtained by using a diphosphine ligand is reported and is formulated $[Cu_6I_6(PPh_2(CH_2)_3PPh_2)_3]$ (**1**). Interestingly, this sort of "eared cubane" cluster based on the $[Cu_6I_6]$ inorganic core can be viewed as a combination of the two known $[Cu_4I_4]$ units, namely, the cubane and the open-chair isomeric geometries. The synthesis, structural and photophysical characterisations, as well as theoretical study of this copper iodide along with the derived cubane (**3**) and open-chair (**2**) $[Cu_4I_4(PPh_3)_4]$ forms, were investigated. A new polymorph of the cubane $[Cu_4I_4(PPh_3)_4]$ cluster is indeed presented (**3**). The structural differences of the clusters were analyzed by solid-state nuclear magnetic resonance spectroscopy. Luminescence properties of the three clusters were studied in detail as a function of the temperature showing reversible luminescence thermochromism for **1** with an intense orange emission at room temperature. This behavior presents different feature compared to the cubane cluster and completely contrasts with the open isomer, which is almost nonemissive at room temperature. Indeed, the thermochromism of **1** differs by a concomitant increase of the two emission bands by lowering the temperature, in contrast to an equilibrium phenomenon for **3**. The luminescence properties of **2** are very different by exhibiting only one single band when cooled. To rationalize the different optical properties observed, density functional theory calculations were performed for the three clusters giving straightforward explanation for the different luminescence thermochromism observed, which is attributed to different contributions of the ligands to the molecular orbitals. Comparison of **3** with its $[Cu_4I_4(PPh_3)_4]$ cubane polymorphs highlights the sensibility of the emission properties to the cuprophilic interactions.
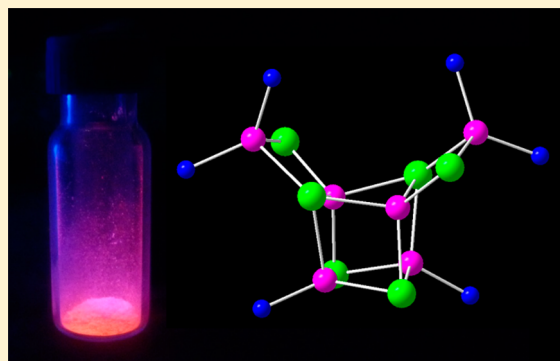
INTRODUCTION

Luminescent materials based on transition-metal complexes have been receiving increasing attention due to their wide field of applications in detection, sensing, biological labeling, and display visualization devices.[1,2] The family of copper(I) halides is particularly attractive owing to its large variety of photophysical properties associated with an extraordinary structural diversity.[3,4] From an economic point of view, copper is also more abundant and less expensive compared to noble metals. In recent years, copper(I) iodide complexes have been intensively studied for

their promising applications in photoactive materials. For example, coordination polymers with potential sensor properties have been reported,[5−7] dinuclear complexes have been successfully tested in OLEDs,[8,9] and tetranuclear clusters have shown pressure-responsive luminescence properties.[10−12] In this context, the development of new copper iodide compounds
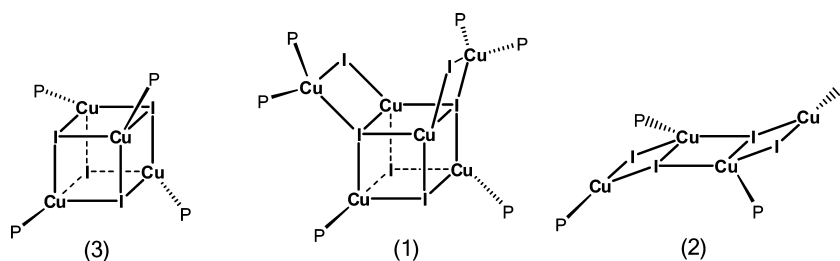
Figure 1. General representation of the copper iodide clusters studied with (**1**) the eared cubane structure, (**2**) the open-chair geometry, and (**3**) the cubane structure. P represents the phosphine ligand.

appears particularly appealing to access original functional materials.

Cooper iodide clusters constitute an interesting class of luminophors exhibiting rich luminescence behavior influenced by the metallophilic interactions. The most popular copper iodide cluster is the cubane compound formulated $[Cu_4I_4L_4]$ (L = organic ligand), which exhibits luminescence thermochromism[13,14] by a variation in temperature of the relative intensities of two emission bands and/or a shift of the emission wavelength, which is correlated to Cu−Cu interactions.[15,16] Different isomers of this cubane cluster exist with the same formula but having different geometries. An isomer with a pseudo octahedral geometry has been reported with phosphine−pyridine ligands.[17−19] A "chair" isomer (also called stairstep structure) also exists, which can be regarded as an open cubane geometry resulting from the breaking of two Cu−I bonds.[20−24] Interestingly these isomers present different photoluminescence behaviors compared to the cubane analogues. Note that in addition to isomers, cubane clusters can also present polymorphism with the same cluster crystallizing in different crystal structures.[12,25−27] The richness of the structural motifs of these clusters due to their geometry flexibility associated with polymorphism allow studying structure-properties relationship giving direct insight into the photophysical properties of these luminophors, which is crucial for their further development.

Here, we report an original copper(I) iodide cluster of novel geometry obtained by using a diphosphine ligand. Interestingly, this sort of "eared cubane" cluster based on the $[Cu_6I_6]$ inorganic core (**1**) can be viewed as a combination of the two known $[Cu_4I_4]$ units; the cubane (**3**) and the open chair (**2**) isomeric geometries (Figure 1). The synthesis, structural and photophysical characterisations, as well as theoretical study of this copper iodide cluster formulated $[Cu_6I_6(PPh_2(CH_2)_3PPh_2)_3]$ are presented. Comparative study with the clusters of derived geometries, namely, $[Cu_4I_4(PPh_3)_4]$ cubane and open forms, was investigated to give insight into the luminescence properties (Chart 1). The structural differences of the clusters were

Chart 1. Designation of the Studied Compounds

$[Cu_6I_6(PPh_2(CH_2)_3PPh_2)_3]$	**1**
$[Cu_4I_4(PPh_3)_4]$ open-chair	**2**
$[Cu_4I_4(PPh_3)_4]$ cubane	**3**

analyzed by ^{63}Cu and ^{31}P solid-state nuclear magnetic resonance (NMR) spectroscopy. For the cubane cluster, a new polymorph of $[Cu_4I_4(PPh_3)_4]$ is presented. Light emission properties of the three clusters were studied in detail as a function of the temperature, showing reversible luminescence thermochromism for the $[Cu_6I_6(PPh_2(CH_2)_3PPh_2)_3]$ cluster with an intense emission at room temperature. This behavior presents different

feature compared to the cubane $[Cu_4I_4]$ cluster and contrasts with the open isomer, which is nonemissive at room temperature. To rationalize the different optical properties observed, density functional theory (DFT) calculations were performed for the three clusters, giving straightforward explanation for the different thermochromism observed.

■ EXPERIMENTAL SECTION

Synthesis. All manipulations were performed with standard air-free techniques using Schlenk equipment, unless otherwise noted. Solvents were distilled from appropriate drying agents and degassed prior to use. Copper(I) iodide, triphenylphosphine (PPh₃), 1,3-bis(diphenylphosphino)propane (PPh₂(CH₂)₃PPh₂ or dppp) were purchased from Aldrich and used as received.

[Cu₆I₆(PPh₂(CH₂)₃PPh₂)₃] (1). 1,3-bis(diphenylphosphino)propane (1.1 g, 2.6 mmol) was added to a suspension of CuI (1 g, 5.3 mmol) in dichloromethane (50 mL). The solution was stirred for 12 h at room temperature. The solution was filtered and evaporated to dryness. The white solid was recrystallized in dichloromethane, and colorless crystals were obtained. Yield = 67% (1.5 g, 0.59 mmol). ^{1}H NMR (300 MHz, CDCl₃): δ (ppm) 7.73–7.26 (m, C₆H₅), 2.38 (br, CH₂P), 1.85 (br, CH₂); ^{31}P NMR (300 MHz, CDCl₃): δ (ppm) −13.2 (br). Anal. Calcd (% wt) for C₈₁H₇₈P₆Cu₆I₆ + 2(CH₂Cl₂): C, 39.10; H, 3.24; Found: C, 38.79; H, 3.11.

[Cu₄I₄(PPh₃)₄] (3). Triphenylphosphine (0.7 mg, 2.6 mmol) was added to a suspension of CuI (0.5 g, 2.6 mmol) in toluene (50 mL). The solution was stirred for 12 h at 110 °C. The solution was filtered, and after it cooled to −4 °C the product was recovered as colorless bulk crystals. Yield = 53% (0.65 g, 0.34 mmol). ^{1}H NMR (300 MHz, CDCl₃): δ (ppm) 7.58–7.17 (m, C₆H₅); ^{31}P NMR (300 MHz, CDCl₃): δ (ppm) −21.9 (br). Anal. Calcd (% wt) for C₇₂H₆₀P₄Cu₄I₄: C, 47.75; H, 3.34; Found: C, 47.86; H, 3.46.

[Cu₄I₄(PPh₃)₄] (2). Powder of **3** (0.5 g, 0.28 mmol) was dissolved in dichloromethane at room temperature. Colorless crystals were obtained from this reaction by allowing the solution to stand at room temperature. Yield = 81% (0.43 g, 0.23 mmol). ^{1}H NMR (300 MHz, CDCl₃): δ (ppm) 7.72–7.29 (m, C₆H₅). Anal. Calcd (% wt) for C₇₂H₆₀P₄Cu₄I₄: C, 47.75; H, 3.34 and for C₇₂H₆₀P₄Cu₄I₄ + 1 (CH₂Cl₂): C, 46.25; H, 3.30; Found: C, 47.17; H, 3.38.

Characterizations. ^{1}H and ^{31}P liquid NMR spectra were recorded on a Bruker Avance II spectrometer at room temperature, operating at the radio frequency (rf) of 300 MHz. ^{1}H spectra were internally referenced from peaks of residual protons in deuterated solvents or from tetramethylsilane (TMS). A solution of H₃PO₄ 85% weight was used as an external standard for ^{31}P spectra. Elemental analyses (C, H) were performed by the Service de microanalyse de l'ICSN - CNRS Gif-sur-Yvette.

The static ^{63}Cu NMR spectra were recorded on a Bruker Avance III 900 MHz spectrometer (B_0 = 21.1 T) using the wideband uniform rate and smooth truncation[28] Carr−Purcell Meiboom−Gill[29] (WURST-Q-CPMG)[30] pulse sequence in static conditions, with an interpulse delay of 202 µs. The WURST pulse had a length of 25 µs and a sweep of 1 MHz under. ^{1}H spinal64[31] decoupling (8 µs pulse with 60 kHz rf field) was applied during acquisition. The recycle delay was 1 s. Number of transients was 40 960, 40 960, and 4096 and number of echoes was 23,
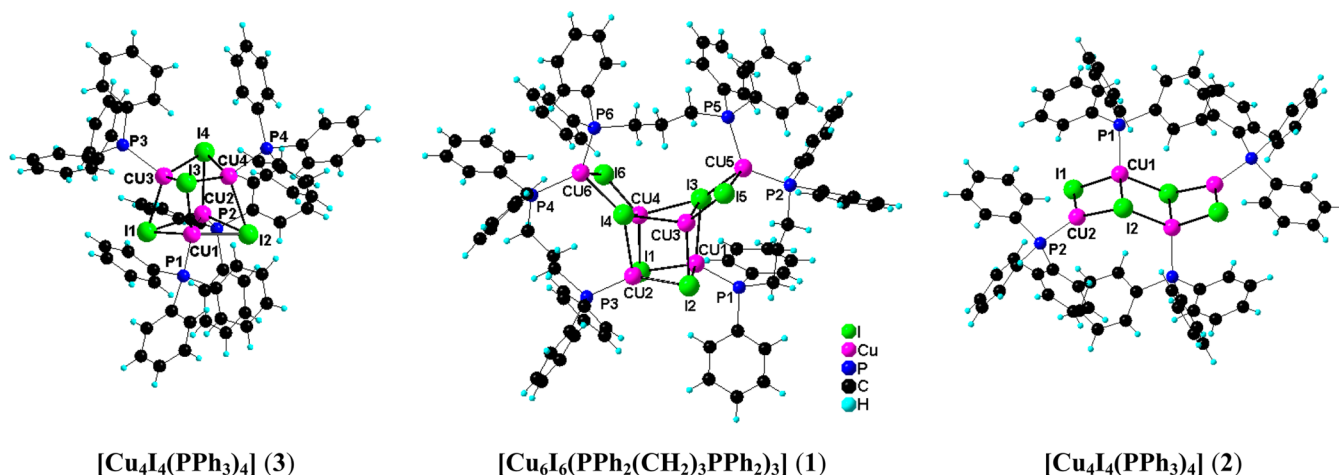
Figure 2. Molecular structures of clusters **1**–**3**.

85, and 85 for **1**, **2**, and **3**, respectively. The chemical shifts were referenced to CuI at 0 ppm. The samples were packed in 2.5 mm outer diameter rotors.

The magic-angle spinning (MAS) ^{1}H NMR spectra were recorded on a Bruker Avance III 900 MHz spectrometer ($\mathbf{B}_0$ = 21.1 T) at MAS of 60 kHz (1.3 mm rotors) using a DEPTH^{32} pulse sequence to suppress the probe background. 1.2 μs $\pi/2$ pulse durations were used. The recycle delay was 5 s, and 64 transients were accumulated for each sample. The chemical shifts are referenced to TMS.

The ^{13}C and ^{31}P cross-polarization (CPMAS) NMR spectra were recorded on an Avance Bruker 500 spectrometer ($\mathbf{B}_0$ = 11.7 T). The samples were packed in 3.2 or 4 mm outer diameter rotors and spun at 10 kHz. The ^{13}C chemical shifts were referenced to TMS at 0 ppm. The ^{31}P chemical shifts were reference to a solution of H_3PO_4 at 0 ppm. ^{1}H SPINAL-64 decoupling was applied during the signal acquisition. The recycle delay was set to 5–20 s, depending on the sample, with 64 to 128 accumulated transients.

Luminescence spectra were recorded on a SPEX Fluorolog FL 212 spectrofluorimeter (Horiba Jobin Yvon). The excitation source is a 450 W xenon lamp; excitation spectra were corrected for the variation of the incident lamp flux, as well as emission spectra for the transmission of the monochromator and the response of the photomultiplier (Peltier cooled Hamamatsu R928P photomultiplier). Low-temperature measurements were done with a liquid helium circulation cryostat SMC TBT Air Liquid model C102084. The absolute internal quantum yields (QY) were measured by using a Fluoromax-4 Horiba Jobin Yvon integrating sphere. Emission lifetimes (τ) were recorded with an Edinburgh Instruments spectrofluorimeter FLS900 equipped with a nanoflash H$_2$ lamp (0.39 bar) using the time-correlated single-photon counting method. Data were analyzed by exponential curve fitting and are reported in Supporting Information.

UV–visible absorption spectra were recorded with a Varian Cary 50 spectrophotometer with dichloromethane solutions of the clusters (c = 1.2 × 10^{-4} mol L^{-1}).

Powder X-ray diffraction (PXRD) diagrams were recorded on a X'Pert Philips diffractometer (40 kV, 40 mA) with Cu Kα radiation (λ = 0.154 056 nm). The calculated diagram obtained from the single-crystal data was obtained with the Mercury software.

Single-crystal XRD analyses were performed to determine the crystalline structures. Suitable single crystals were obtained for clusters **1**–**3** as described in the Synthesis Section. Crystals were mounted on Kapton loop using paratone oil and immediately cooled in a cold stream of nitrogen. All data were collected on a Nonius Kappa CCD diffractometer using Mo Kα (λ = 0.710 73 Å) X-ray source and a graphite monochromator. The cell parameters were initially determined using more than 50 reflections. Experimental details are described in Supporting Information, Table S1. The crystal structures were solved with SIR 97^{33} and refined in SHELXL-97^{34} by full-matrix least-squares using anisotropic thermal displacement parameters for all non-hydrogen

atoms. All the hydrogen atoms were placed in geometrically calculated positions. Details of crystal data and structure refinements are summarized in Table S1.

Computational Details. Density functional theory (DFT) calculations were carried out with the program Gaussian09,^{35} using the PBE1PBE (PBE0)^{36} functional and a standard double-ξ polarized basis set, namely, the LANL2DZ set,^{37} augmented with polarization functions on all atoms, that is, a p orbital with exponent 0.8 for H, a d orbital with exponents 0.8, 0.55, and 0.309 for C, P, and I, respectively, and an f orbital with exponent 0.8 for Cu. Spin-unrestricted calculations were performed in the case of triplet states. Vibrational frequency calculations were performed on all the optimized structures to ascertain they are minima on the potential energy surface. Calculations on cluster **3** have already been published.^{16} Its major results are discussed here for the sake of comparison with **1** and **2**. The ground-state optimized geometries of compounds **1**, **2**, and **3** are of C_1, C_i, and T symmetry, respectively. Calculations including solvent effect using the polarizable continuum model (PCM)^{38} were also performed for **1**, **2**, and **3**.

The composition of the molecular orbitals was calculated using the AOMix program.^{39} The UV–visible transitions were calculated by means of time-dependent DFT calculations^{40} at the same level of theory. The 80 singlet–singlet transitions of lowest energy were computed for **1**, **2**, and **3**. This corresponds to wavelengths larger than 276, 204, and 248 nm, respectively. Only transitions with oscillator strengths larger than or equal to 0.02, 0.05, and 0.02 for **1**, **2**, and **3**, respectively, are reported and discussed. Representations of the molecular structures were done using the program MOLEKEL 4.3.^{41}

The NMR parameters were computed assuming the gauge-independent atomic orbital method,^{42} using the same PBE1PBE (PBE0)^{36} functional, but with the all-electron triple-ζ polarized Def2-TZVP basis set from the EMSL Basis Set Exchange Library.^{43} Electric field gradients and NMR shielding tensors were computed from single-point calculations of **1** on the molecular geometries taken from the X-ray structure in which the hydrogen atoms were relocated at calculated positions assuming C–H distances of 1.08 Å. As the structure is disordered, the calculations were performed on both forms. However, as the disorder does not concern the cluster core, the differences between the two forms are small (Supporting Information, Table S11), and the calculated spectra are almost indistinguishable (Supporting Information, Figure S11). Quadrupolar moments of −0.220 and −0.204 × 10^{-28} m^2 were considered for ^{63}Cu and ^{65}Cu, respectively. The results were analyzed with the help of the EFGshield program.^{44} The ^{65}Cu NMR spectra were finally simulated using the Dmfit^{45} software.

■ RESULTS AND DISCUSSIONS

Synthesis and X-ray Diffraction Characterization. Clusters **1** and **3** were synthesized in dichloromethane and toluene, respectively, from CuI and the corresponding

Table 1. Selected Bonds Lengths (Å) and Angles (deg) in Clusters 1−3 at 150 K

compound	$[Cu_4I_4(PPh_3)_4]$ (**3**)	$[Cu_6I_6(PPh_2(CH_2)_3PPh_2)_3]$ (**1**)	$[Cu_4I_4(PPh_3)_4]$ (**2**)
Cu−Cu	Cu2−Cu1 2.768(1)	Cu3−Cu1 2.756(1)	Cu1−Cu2 2.771(1) × 2
	Cu3−Cu4 2.863(1)	Cu3−Cu4 2.855(1)	Cu1−Cu1 3.424(1)
	Cu3−Cu2 2.880(1)	Cu4−Cu2 2.894(1)	
	Cu4−Cu2 2.900(1)	Cu2−Cu1 3.065(1)	
	Cu3−Cu1 2.964(1)	Cu4−Cu1 3.154(0)	
	Cu4−Cu1 3.030(1)	Cu3−Cu2 3.242(0)	
		Cu6−Cu4 3.275(1)	
		Cu5−Cu3 3.415(1)	
mean	2.901(1)	3.082(1)	2.989(1)
Cu−I	Cu1−I2 2.6495(6)	Cu4−I6 2.5947(6)	Cu2−I1 2.5396(6)
	Cu3−I3 2.6496(6)	Cu3−I5 2.6099(6)	Cu2−I2 2.5917(7)
	Cu4−I4 2.6524(6)	Cu4−I4 2.6399(7)	Cu1−I1 2.6412(7)
	Cu2−I1 2.6562(6)	Cu2−I2 2.6406(6)	Cu1−I2 2.7080(6)
	Cu1−I1 2.6826(6)	Cu2−I1 2.6512(7)	Cu1−I2 2.7060(6)
	Cu3−I1 2.6856(6)	Cu6−I6 2.6643(6)	
	Cu3−I4 2.6915(6)	Cu1−I1 2.6643(6)	
	Cu2−I2 2.6934(6)	Cu3−I3 2.6732(6)	
	Cu2−I4 2.7043(6)	Cu5−I5 2.6740(6)	
	Cu1−I3 2.7113(6)	Cu3−I2 2.6812(6)	
	Cu4−I2 2.7153(6)	Cu1−I2 2.7052(6)	
	Cu4−I3 2.7293(6)	Cu4−I1 2.7120(6)	
		Cu3−I4 2.7376(7)	
		Cu4−I3 2.7406(7)	
		Cu1−I3 2.7416(6)	
		Cu5−I3 2.8090(6)	
		Cu6−I4 2.8614(6)	
		Cu2−I4 2.8857(6)	
mean	2.6851(6)	2.7048(7)	2.6373(7)
Cu−P	Cu2−P2 2.254(1)	Cu1−P1 2.247(1)	Cu2−P2 2.231(1) × 2
	Cu1−P1 2.255(1)	Cu2−P3 2.252(1)	Cu1−P1 2.240(1) × 2
	Cu3−P3 2.256(1)	Cu5−P2 2.252(1)	
	Cu4−P4 2.263(1)	Cu5−P5 2.258(1)	
		Cu6−P6 2.272(1)	
		Cu6−P4 2.283(1)	
mean	2.257(1)	2.261(1)	2.236(1)
I−Cu−I	I2−Cu4−I3 104.64(2)	I2−Cu2−I4 95.41(2)	I2−Cu1−I2 101.55(2) × 2
	I2−Cu1−I3 106.98(2)	I1−Cu4−I3 97.77(2)	I1−Cu1−I2 104.27(2) × 2
	I1−Cu1−I3 106.25(2)	I2−Cu3−I4 98.04(2)	I1−Cu1−I2 112.23(2) × 2
	I3−Cu3−I1 107.95(2)	I5−Cu5−I3 98.62(2)	I1−Cu2−I1 119.87(2) × 2
	I2−Cu2−I4 108.97(2)	I1−Cu1−I3 98.90(2)	
	I1−Cu3−I4 108.56(2)	I6−Cu6−I4 100.81(2)	
	I1−Cu2−I4 109.05(2)	I5−Cu3−I3 103.83(2)	
	I4−Cu4−I2 109.86(2)	I1−Cu1−I2 106.19(2)	
	I4−Cu4−I3 111.95(2)	I2−Cu2−I1 108.47(2)	
	I3−Cu3−I4 113.25(2)	I6−Cu4−I3 108.48(2)	
	I1−Cu2−I2 114.34(2)	I6−Cu4−I4 108.93(2)	
	I2−Cu1−I1 114.93(2)	I5−Cu3−I2 110.28(2)	
		I6−Cu4−I1 110.68(2)	
		I3−Cu3−I4 111.00(2)	
		I4−Cu4−I3 111.93(2)	
		I1−Cu2−I4 112.15(2)	
		I5−Cu3−I4 114.51(2)	
		I2−Cu1−I3 116.42(2)	
		I4−Cu4−I1 118.35(2)	
		I3−Cu3−I2 119.69(2)	
mean	109.73(2)	108.39(2)	109.48(2)

phosphine ligands (PPh$_2$(CH$_2$)$_3$PPh$_2$ or PPh$_3$). **2** was obtained by recrystallizing **3** in dichloromethane. All compounds were obtained as colorless crystals (Experimental Section), and the

crystal structures were determined by single-crystal XRD analysis at 150 K. In all the structures, solvent molecules are included, and the formulas are [Cu$_6$I$_6$(PPh$_2$(CH$_2$)$_3$PPh$_2$)$_3$]·2 CH$_2$Cl$_2$ (**1·2**

CH_2Cl_2), $[Cu_4I_4(PPh_3)_4] \cdot CH_2Cl_2$ (**2**·CH_2Cl_2), and $[Cu_4I_4(PPh_3)_4] \cdot 2.5C_7H_8$ (**3**·$2.5C_7H_8$). These formulations are in agreement with NMR (^1H and ^{31}P) and elemental analyses. Note that the synthesis of **2** has been already reported in the literature by refluxing CuI and PPh_3 in chloroform[22] or by mechanosynthesis method.[27] In the former case, a crystal structure of **2** has been determined but without solvent included. Two polymorphs of the cubane cluster $[Cu_4I_4(PPh_3)_4]$ are known, which crystallize in the monoclinic $P2_1/c$ (**3P**)[16] and cubic I-$43d$ space groups.[25] Here, another third polymorph was therefore obtained (**3**), with toluene molecule included in the crystalline structure. However, after few days in air, the crystals of **3** are converted into the monoclinic unsolvated polymorph (**3P**) as revealed by the X-ray diffraction powder diagram and elemental analysis (Supporting Information).

Both **1** and **3** clusters crystallize in the monoclinic $P2_1/c$ space group, whereas **2** crystallizes in the $C2/c$. The unit cell contents are shown in Supporting Information, Figure S1. All three structures can be described as assembly of columns of clusters. For **1**, the columns of clusters are along the c axis, and the cluster orientation changes alternatively along the chain (up and down). For **3**, the columns run along the b axis. For **2**, the columns are along the c axis, and the orientation of the cluster changes from one chain to the other. The molecular structures of the clusters are depicted in Figure 2. Cluster **3** presents a classical cubane structure formed by four copper atoms and four iodine atoms that occupy alternatively the corners of a distorted cube. The phosphine ligands are coordinated to each copper atom by the phosphorus atom. The copper atoms have all a tetrahedral CuI_3P environment. In cluster **2**, this cubane structure is open (two Cu−I bonds fewer) forming a chair configuration. In this case, two copper atoms have a tetrahedral CuI_3P environment, and the two others have a planar CuI_2P configuration. Cluster **1** presents a $[Cu_6I_6]$ inorganic core, which can be described as the fusion of a cubane and an open $[Cu_4I_4]$ unit. In other words, the $[Cu_4I_4]$ cubane structure was extended by two [CuI] moieties forming a sort of eared cubane. Three diphosphine dppp ligands coordinate the $[Cu_6I_6]$ core in bidente mode with two disordered phenyl groups (not shown in Figure 2). All six copper atoms have a tetrahedral environment, two with CuI_3P, two others with CuI_2P_2, and the remaining two with CuI_4 configuration.

Selected bond lengths and angles of the clusters are listed in Table 1. The ligands present a classical geometry for phosphine-based copper iodide clusters. The Cu−P values are similar for clusters **1** and **3** and are slightly shorter for **2**. This shortening can be attributed to steric hindrance of the groups bonded to the phosphorus atoms as observed in the literature for $[Cu_4I_4(P-(NMe_2)_3)_4]$ (mean 2.231 Å).[46] The Cu−I bond distances are also shorter in **2** compared to **1** and **3**. The I−Cu−I angle mean values for all the clusters are comparable and within the range of reported values for this type of cluster with phosphine ligands. **2** has two short Cu−Cu bond lengths (2.771(1) Å) and one longer bond (3.424(1) Å) at the center of the compound. Considering the van der Waals radii of copper(I) (1.40 Å),[47] weak metal−metal (d^{10}−d^{10}) bonding interactions occur in this cluster between the two $[Cu_2I_2]$ units within there are significant metallic interactions.[48] Cuprophilic interactions are also present in cluster **3** with mean Cu−Cu distances of 2.901(1) Å. Comparable and slightly longer distances are found in cluster **1** (mean 3.082(1) Å) with the two longer ones in the extended [CuI] ear units (3.275(1) and 3.415(1) Å).

Solid-State Nuclear Magnetic Resonance Analysis. The clusters were characterized by solid-state NMR spectroscopy.

The unsolvated form of **3** (polymorph **3P**) was studied instead of **3** to prevent conversion during the experiment. The ^1H and ^{13}C CPMAS NMR spectra of **1**−**3** are reported in Supporting Information and are in agreement with the corresponding ligands. The ^{31}P and ^{63}Cu NMR spectra are reported in Figures 3
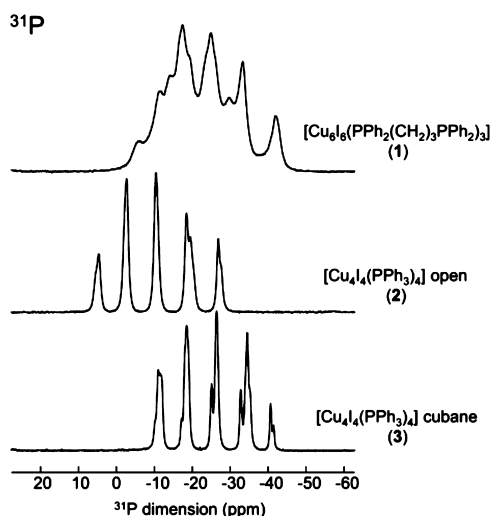
Figure 3. ^{31}P CPMAS NMR spectra of **1**−**3**.
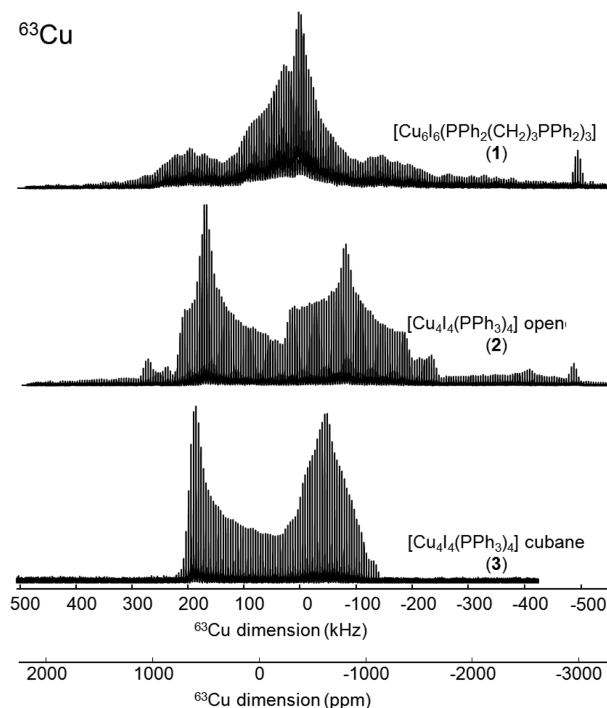
Figure 4. Static ^{63}Cu solid-echo NMR spectra of **1**−**3**. The peaks at −500 ppm are the copper signal of the NMR coil.

and 4, respectively. The ^{31}P solid-state CPMAS NMR spectra of **2** and **3** are in agreement with previous reports (unsolvated forms).[21] They present several combinations of quartets resulting from the one-bond J-couplings between the ^{31}P and the two copper isotopes (^{65}Cu, with 30.8% natural abundance and ^{63}Cu, with 69.2% natural abundance, both having a nuclear spin value of 3/2). For **2**, the spectrum is composed of two

quartets from the two independent P atoms in the structure,[49] whereas for **3** there are four (Supporting Information, Figure S12). For **1**, because of the six independent phosphorus atoms in the structure, the six quartets are so overlapped that they are hardly distinguishable. However, one can notice that the chemical shift values (taken as the barycenters of the NMR patterns) of **1** (−25 ppm) and **3** (−22 ppm) are similar but are different from **2** (−12 ppm), which can be attributed to the different coordination modes of the Cu atoms. All are indeed four-coordinated in **1** and **3**, whereas in **2** two are three-coordinated.

The less common ^{63}Cu NMR nucleus was also studied. ^{63}Cu (nuclear spin 3/2) is sensitive and reasonably abundant (69.2%) but has a large quadrupolar moment,[28−30] which, as shown in Figure 4, results in particularly broad NMR patterns extending over a megahertz, even at high magnetic field (21.1 T). The ^{63}Cu NMR patterns are clearly distinct for the three clusters. The spectra of the chair (**2**) and cubane (**3**) $[Cu_4I_4(PPh_3)_4]$ isomers are similar to those previously reported,[49,12] although these were recorded at lower magnetic fields. The NMR spectrum of the new compound **1**, despite its apparent complexity, can be understood with the help of DFT calculations of the ^{63}Cu shielding and quadrupolar coupling tensors reported in Supporting Information (the results for **2** and **3** have been reported elsewhere[49,12]). Although slightly overestimated for all sites (as was also observed for **3**), the calculated values closely reproduce the overall shape of the experimental ^{63}Cu NMR spectrum. These values were used as starting point to further refine the experimental quadrupolar parameter values (keeping the chemical shielding and asymmetry parameters as calculated, see Supporting Information) and to assign the resonances to the corresponding crystallographic copper sites. In **3**, moderate quadrupolar coupling constant (C_Q) have been observed (i.e., ca. 10−15 MHz) for the four-coordinated copper atoms.[12] In **2**, the copper is three- and four-coordinated, the former having a much larger C_Q value (∼50 MHz) than the latter (∼20 MHz).[49] In **1**, although the Cu atoms are all four-coordinated, three ranges of ^{63}Cu C_Qs are observed: Cu(1) and Cu(2) (both CuI$_4$) have moderate C_Q values of ∼10 MHz, as observed in the cubane clusters, Cu(5) and Cu(6) (both CuI$_2$P$_2$) have larger values of ∼22 MHz, as observed in **2**, while Cu(3) and Cu(4) (both CuI$_3$P) have much smaller values of 6−7 MHz. It is therefore very interesting to note the sensitivity of the ^{63}Cu C_Q parameters not only to the coordination number of the copper atoms (three or four) but also to the nature of the first neighbors (I or P).

Optical Properties. Clusters **1**−**3** are white powders under ambient light. At room temperature, under UV irradiation, **1** and **3** emit an intense orange and green light, respectively, whereas **2** is nonemissive (Figure 5). The luminescence thermochromism of clusters **1** and **3** is revealed by dipping the samples into liquid nitrogen; the orange emission is replaced by a purple one, and the green emission is replaced by a blue one. Cluster **2** becomes emissive at low temperature with a sky-blue light. When the samples are progressively warmed to room temperature, the original emissions are recovered, indicating a completely reversible thermochromic luminescence for the clusters.

Solid-state emission and excitation spectra were recorded for clusters **1**−**3** from room temperature to 8 K (Figures 6−8), and corresponding data are reported in Table 2. At 285 K, the emission spectra display a single unstructurated broad emission band, namely, low energy (LE), centered at 655 nm (λ_{ex} = 290 nm) for **1** and at 535 nm (λ_{ex} = 300 nm) for **3** in agreement with the orange and green light observed, respectively. At 280 K,

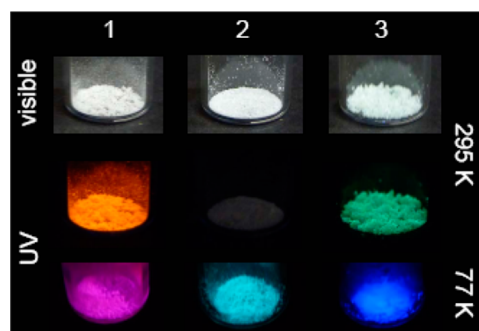**Figure 5.** Photos of powder of clusters **1**−**3** under UV irradiation at 312 nm (UV lamp) at room temperature (295 K) and in liquid nitrogen (77 K).
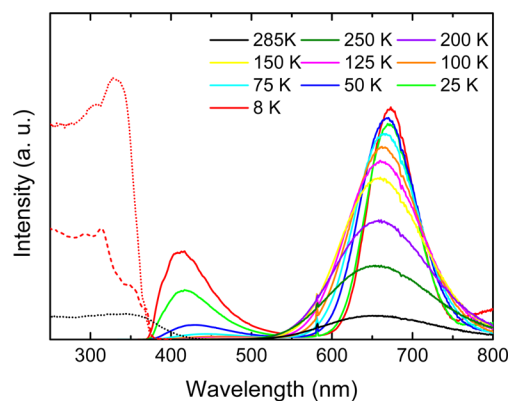

Figure 6. Temperature dependence of solid-state luminescence spectra of **1** with emission spectra from 285 to 8 K at λ_{ex} = 290 nm and excitation spectra at λ_{em} = 660 nm (red and black dotted lines) and at λ_{em} = 420 nm (red dashed lines). The peak at 580 nm is due to the partial filter cutoff of the second harmonic excitation.
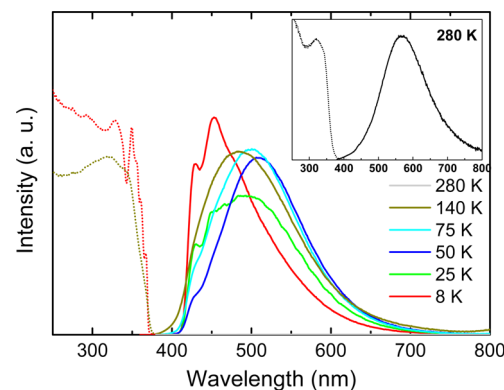
Figure 7. Temperature dependence of solid-state luminescence spectra of **2** with emission (solid line) from 280 to 8 K at λ_{ex} = 325 nm and excitation spectra at λ_{em} = 450 nm (red dotted lines) and at λ_{em} = 500 nm (dark-yellow dotted lines). (inset) Emission and excitation (λ_{em} = 560 nm) spectra at 280 K.

cluster **2** presents a weak emission at 568 nm (λ_{ex} = 325 nm). This agrees with the very low absolute internal quantum yield determined at room temperature for **2** (<1%) compared to those of **1** and **3** with 39 and 91%, respectively (λ_{ex} = 330 nm).

By lowering the temperature, a new emission band (high energy (HE)) appears at higher energy for clusters **1** and **3**. At 8 K, the two bands of **1** are centered at 413 and 673 nm (Figure 6). At 75 K, the combination of the blue band with the red one leads
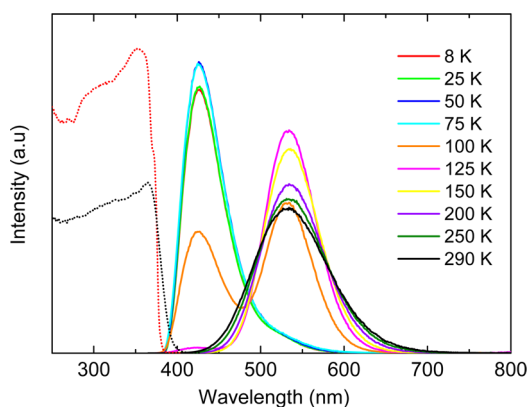
Figure 8. Temperature dependence of solid-state luminescence spectra of **3** from 290 to 8 K with emission at $\lambda_{ex} = 300$ nm (solid lines) and excitation spectra at $\lambda_{em} = 425$ nm (red dotted lines) and at $\lambda_{em} = 535$ nm (black dotted lines).

Table 2. Photoluminescence Data at Different Temperatures of Clusters 1−3

compound	T (K)	$\lambda_{em}^{max} [\lambda_{ex}]^a$ (nm)
$[Cu_6I_6(PPh_2(CH_2)_3PPh_2)_3]$ (**1**)	285	655 [290]
	125	661 [290]
	75	665 [290] (1)
		443 [290] (0.03)
	8	673 [290] (1)
		413 [290] (0.4)
$[Cu_4I_4(PPh_3)_4]$ (**2**)	280	568 [325]
	140	485 [325]
	75	500 [325]
	8	454 [325]
$[Cu_4I_4(PPh_3)_4]$ (**3**)	290	535 [300]
	100	535 [300] (1)
		425 [300] (0.8)
	8	425 [300]

^{a}In brackets are reported the relative intensities of the LE and HE emission bands.

to the purple emission observed in liquid nitrogen (Figure 5). The intensity of the two bands increases concomitantly when the sample is cooled and is for the LE one accompanied by a red shift (18 nm) and a narrowing of the bandwidth. The excitation profiles of the two emission bands are similar with maxima at 330 nm. For cluster **3**, the HE band progressively increases in intensity, but in this case, this is concomitant with the extinction of the green LE band (Figure 8). At 100 K, the two emission bands are present with maxima at 425 and 535 nm. At 75 K, the HE band is predominant in agreement with the blue emission observed in liquid nitrogen (Figure 5). In this case, there is no band shifting associated with the relative change of intensity of the two emission bands. The Stokes shift between excitation and emission maxima of the LE band, 19 620 and 14 640 cm^{-1} for clusters **1** (at 8 K) and **3** (at 100 K), respectively, are thus much larger compared to those of the HE band 10 270 and 7800 cm^{-1}. The luminescent behavior of cluster **2** contrasts with that of **1** and **3** with a single emission band. As shown in Figure 7, the weak room-temperature emission band increases in intensity by lowering the temperature. At 8 K the band maximum is at 454 nm ($\lambda_{ex} = 325$ nm), and a kind of vibronic structure can be distinguished. The position of the band varies significantly with the temperature (red shift from 140 to 50 K and then blue shift to

8 K). The excitation profile of the emission band at 8 and 140 K presents different features. The weak luminescence and the emission blue shift at low temperature have been already reported for the unsolvated form of **2**.[27] Emission lifetimes were determined for **1** and **3** clusters at room temperature, whereas for **2** the intensity was too low for an accurate measurement (corresponding decays are reported in Supporting Information). Cluster **1** presents a biexponential decay with $\tau_1 = 0.7$ and $\tau_2 = 3.2$ μs (57%), and **3** has a single one with $\tau = 4.2$ μs.

Density Functional Theory Calculations. *Relative Isomer Stability.* We first address the question of the relative stability of **2** and **3**, which are two isomers of $[Cu_4I_4(PPh_3)_4]$, both synthesized at room temperature in different solvents (toluene and dichloromethane). DFT calculations considering the solvent effect (PCM calculations) were thus performed to evaluate their relative stability. Solvents of increasing polarity, namely, toluene, chloroform, dichloromethane, and acetonitrile, were considered. The optimized metrical data are in fair agreement with experiment, with a slight overestimation (3−4%) of the bond distances. (Supporting Information, Tables S2 and S3). For both isomers, the Cu−Cu and Cu−I distances increase with solvent polarity, whereas the Cu−P, C−P, and C−C distances do not vary significantly. As far as total energy (ΔE_0) is considered, **3** is found to be more stable than **2** in any solvent (Table 3).

Table 3. Relative Energy of 2 with Respect to That of 3 in Vacuum and Various Solvents

	ΔE_0 (kcal/mol)^a	ΔG (kcal/mol)^b
vacuum	9.2	−1.6
toluene	6.9	−3.2
chloroform	5.8	−3.0
dichloromethane	5.1	1.2
acetonitrile	9.5	5.3

^{a}Including ZPVE contribution. ^{b}Free energy at 298 K.

However, the energy difference is quite small, in apparent contradiction with the fact that **2** has two fewer Cu−I bonds than **3**. This is because **2** has less strain constraints and therefore compensates its lower number of bonds by stronger bonds. When free energy (ΔG) is considered, the difference between **2** and **3** is even reduced (Table 3), due to entropic effects, and **2** is found slightly more stable than **3** in vacuum, toluene, and chloroform. These results are consistent with the fact that **2** and **3** are obtained from toluene and dichloromethane solutions, respectively. This nearly iso-energetical nature found for **2** and **3** is also consistent with the general observation of isomerism within the $[Cu_4I_4L_4]$ family.

Ground and Excited States of Clusters 1−3 in Relation with Their Optical Properties. The results reported below concern optimized geometries of isolated molecules (see Computational Details) and therefore neglect the solid-state packing effects and the possible differences between polymorphs. The geometries of the singlet ground state (S_0, Figure 9) and of the lowest triplet state (T_1) were optimized for the three compounds. A second lowest triplet state (T_2) was also optimized in the case of compounds **1** and **3**.[16] Relevant computed data for all these states (S_0, T_1, and T_2) are reported in Table 4 along with the experimental metrical data (X-ray analysis data in brackets). The computed values are in a satisfying agreement with the experimental ones. The electronic transitions of lowest energy were also calculated by the TD-DFT method. The corresponding calculated absorption and emission wavelength values are given
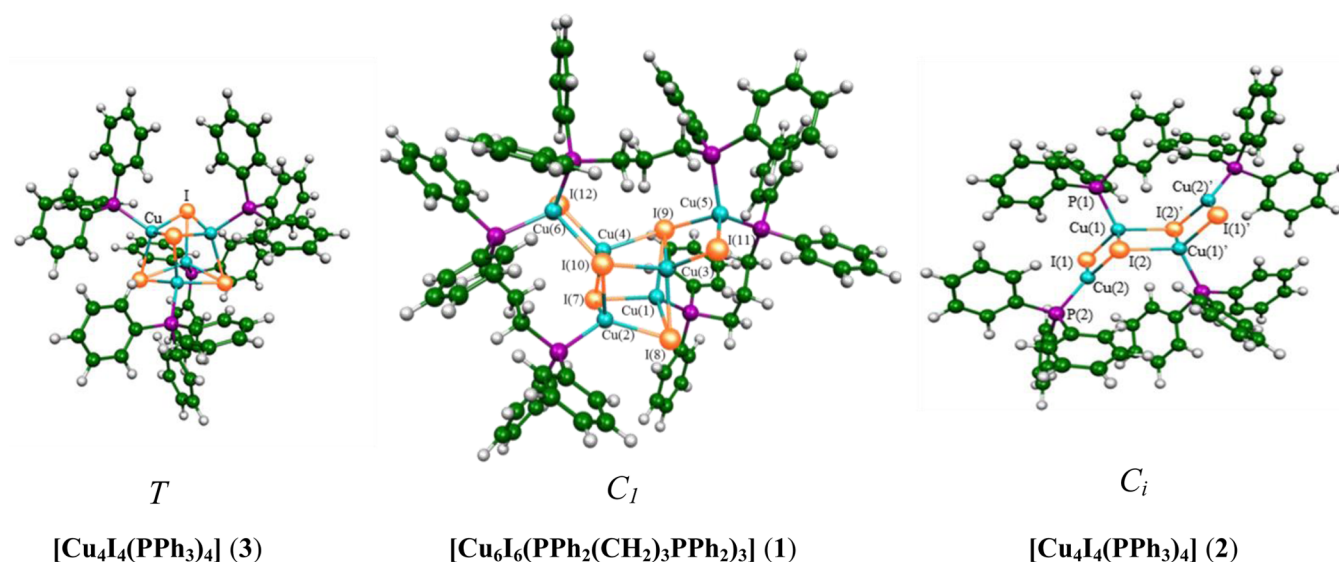
Figure 9. Optimized geometries of the S_0 ground state of **1−3** in C_1, C_i, and T symmetries, respectively.

Table 4. Relevant Computed Data for 1−3

	[Cu$_6$I$_6$(PPh$_2$(CH$_2$)$_3$PPh$_2$)$_3$]^a (1)			[Cu$_4$I$_4$(PPh$_3$)$_4$]^a open (2)		[Cu$_4$I$_4$(PPh$_3$)$_4$]^a cubane (3)[16]		
	S_0 (C_1)	T_1 (C_1)	T_2 (C_1)	S_0 (C_i)	T_2 (C_1)^b	S_0 (T)	T_1 (C_2)	T_2 (C_1)
relative energy (eV)	0.00	2.86	3.32	0.00	3.22	0.00	3.29	3.38
Cu−Cu (Å)								
range	2.793−3.198	2.522−3.479	2.801−3.219	2.869	3.099	3.040	2.576−2.666	2.941−3.035
	[2.756−3.415]	2.817	2.996	[2.771]	3.238	[2.776−3.100]	2.635	
mean	2.992			3.153		3.040		3.016
	[3.082]			[3.424]		[2.901]		
Cu−I (Å)								
range	2.656−2.905	2.593−3.795	2.652−2.930	2.540−2.706	2.645−2.867	2.740	2.806−3.145	2.680−2.760
	[2.595−2.886]	2.888	2.741	[2.598−2.749]	2.742	[2.650−2.712]	2.916	
mean	2.742			2.691		2.740		2.725
	[2.705]			[2.637]		[2.684]		
Cu−P (Å)								
range	2.336−2.374	2.325−2.366	2.336−2.374	2.318−2.342	2.315−2.368	2.357	2.368−2.380	2.34−2.37
	[2.254−2.270]	2.352	2.358	[2.231−2.240]	2.344	[2.258−2.253]	2.374	2.355
mean								
	2.354			2.330		2.357		
	[2.261]			[2.236]		[2.255]		

^{a}Values in brackets are the X-ray experimental data. ^{b}T$_2$ is the lowest computed triplet state of **2**; no T$_1$ (^{3}CC cluster centered) state could be found (see text).

in Table 5 along with the experimental ones for the sake of comparison. The UV−visible absorption spectra of clusters **1−3** recorded in dichloromethane are shown in the Supporting Information. The emission wavelengths were calculated as the difference between the energy of the optimized excited triplet state and the energy of the singlet ground state assuming the same (unrelaxed) geometry as that of the considered triplet state.

Let us first recall the major features of the thermochromic emissive properties of the cubane cluster **3** in the light of its calculated ground and exited states (molecular orbital diagram reported in Supporting Information).[16] The 24 lowest unoccupied orbitals of **3** are combinations of its π^*(phenyl) orbitals and lie in a rather narrow energy range. Promoting an electron from the S_0 nonbonding highest occupied molecular orbital (HOMO, of mixed 3d(Cu)/I character) into one (or a combination of) the π^*(phenyl) orbitals generates the T$_2$ excited state (^{3}X,MLCT transition, Table 5). Just above this block of 24 orbitals lies an in-phase orbital of a symmetry of large copper 4s/4p character, thus strongly metal−metal bonding. Promoting an electron into this orbital generates the T$_1$ excited state (^{3}CC cluster-centered transition, Table 5) and causes a substantial shortening of the Cu−Cu distances (Table 4), which in turn significantly stabilizes this triplet state. At low temperature, the T$_2$ state is populated, responsible for the HE emission. Raising the temperature results in populating T$_1$ from T$_2$ corresponding to the LE emission (Table 4). The thermal equilibrium between T$_2$ and T$_1$ is at the origin of the luminescence thermochromism observed for copper cubane clusters with intensity variation of the HE and LE emission bands.

We now switch to the chair isomer **2**, whose ground-state molecular orbital (MO) diagram is represented in Figure 10. As in the case of **3**, the highest occupied MOs are mainly composed

Table 5. Optical Calculated and Experimental Data for 1−3

compound	$[Cu_6I_6(PPh_2(CH_2)_3PPh_2)_3]$ (1)		$[Cu_4I_4(PPh_3)_4]$ chair (2)		$[Cu_4I_4(PPh_3)_4]$ cubane (3)[16]	
data	exp[a]	calc[a]	exp[a]	calc[a]	exp[a]	calc[a]
absorption λ, nm	300 (broad)	281 (0.02) Cu/I → π*phenyl 4a → 16a (12%) 3a → 16a (11%)	300 (broad)		300 (broad)	
		296 (0.02) Cu/I → π*phenyl 7a → 17a (17%) 6a → 17a (12%)				
		297 (0.03) Cu/I → π*phenyl 5a → 13a (12%) 8a → 17a (12%) 8a → 18a (12%)		271 (0.05) Cu/I → π*phenyl $2a_u → 9a_g$ (+18%) $2a_u → 10a_g$ (+12%) $3a_u → 13a_g$ (12%)		
		301 (0.02) Cu/I → π*phenyl 7a → 18a (13%)		287 (0.05) Cu/I → π*phenyl $2a_g → 7a_u$ (+27%) $3a_u → 9a_g$ (+26%) $3a_u → 8a_g$ (+10%)		282 (0.08) Cu/I → π*phenyl 5t → 3a (57%) 5t → 9t (34%)
		304 (0.04) Cu/I → π*phenyl 8a → 17a (47%)		297 (0.07) Cu/I → π*phenyl $2a_u → 7a_g$ (+32%) $2a_g → 7a_u$ (14%) $2a_u → 5a_g$ (11%)		303 (0.02) Cu/I → π*phenyl 5t → 2a (53%) 5t → 8t (41%)
		306 (0.02) Cu/I → π*phenyl 8a → 13a (22%) 7a → 13a (18%)				313 (0.07) Cu/I → π*phenyl 5t → 2e (42%) 5t → 6t (26%) 5t → 7t (25%)
		307 (0.04) Cu/I → π*phenyl 8a → 15a (28%) 8a → 14a (17%) 7a → 15a (12%)		307 (0.05) Cu/I → π*phenyl $3a_u → 6a_g$ (+41%) $3a_u → 7a_g$ (21%) $2a_u → 3a_g$ (15%)		
		319 (0.02) Cu/I → π*phenyl 7a → 11a (30%) 8a → 11a (26%) 8a → 10a (19%) 7a → 10a (14%)		327 (0.07) Cu/I → π*phenyl $3a_u → 4a_g$ (+79%)		
emission λ, nm	413 (8 K) 655 (290 K)	444 ($T_2 → S_0$) 668 ($T_1 → S_0$)	568 (280 K) 500 (77 K)	499 ($T_2 → S_0$)	405 (8 K) 545 (290 K)	475 ($T_2 → S_0$) 517 ($T_1 → S_0$)

[a]Values in brackets are the oscillator strengths associated with the absorption wavelengths. Only the major contributions to these transitions are indicated with their corresponding weights in %.

of 3d(Cu) and 5p(I) orbitals, and the 24 lowest unoccupied MOs are π*(phenyl) combinations. Significantly above this block of orbitals lies an orbital having a strong copper 4s/4p character ($15a_g$), which is bonding along the Cu_4 zigzag chain. The calculated electronic transition of lowest energy corresponds to an electron promotion from the HOMO to one of the lowest π* combination set (Table 4) so to a mixed ^{1}X,MLCT charge transfer transition (Table 5). The absorption spectrum of cluster 2 (Supporting Information, Figure S7) exhibits a broad band centered at 300 nm, which is in fair agreement with these calculated wavelengths (271−327 nm).

The calculated triplet state of 2 (T_2) corresponds to the occupancy of the π* character lowest unoccupied molecular orbitals (LUMOs, LUMO − LUMO+23). Its optimized geometry (without symmetry constraint) is shown in Figure 11. A dramatic change of the geometry of the copper Cu(2) atom occurred upon excitation. Its trigonal CuI_2P coordination sphere becomes tetrahedral $CuI_2P(\eta^2\text{-CC})$ by the additional coordination of a phenyl carbon−carbon double bond (C(80)═C(82)). In fact, the excited electron goes from the Cu(1)′ atom to the C(79) and C(88) carbon atoms of this phenyl group. This leads

to a weakening of the C(80)═C(82) double bond, which then interacts with the neighboring Cu(2) atom (drastic shortening of the Cu−C distances; see Supporting Information). The calculated density of spin shows that the unpaired electrons are mainly localized on the Cu(2), C(79)−C(88), Cu(1), and P(1) atoms (Supporting Information, Tables S5 and S6).

In the case of 2, the T_1 triplet cannot be stabilized because it is bonding along only three Cu−Cu contacts, compared to six in the more compact cubane isomer 3. The T_1 triplet state is not anymore reachable due to its high energy. Thus, only one emission band is observed for 2, corresponding to the electronic transition $T_2 → S_0$, namely, ^{3}X,MLCT. The corresponding calculated value of 499 nm (Table 5) is in a rather good agreement with the corresponding experimental one (568 nm at 290 K) especially at low temperature (500 nm at 77 K). This leads to the lack of luminescence thermochromism for 2 with one single emission band in contrast to 3. The low intensity of the emission band at room temperature can be explained by nonradiative phenomenon induced by the ligand flexibility.

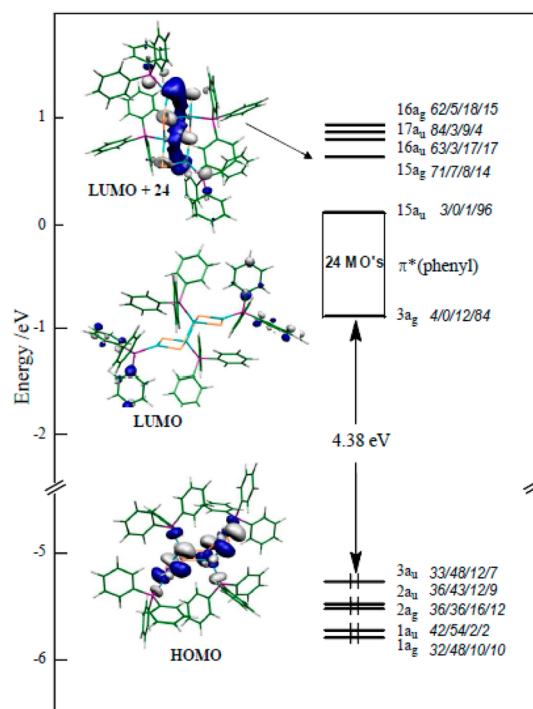The ground-state electronic structure of cluster 1 was calculated, and its MO diagram is represented in Figure 12.

Figure 10. MO diagram of **2** in its ground state. The MO localizations (in %) are given in the following order: Cu/I/P/phenyl.
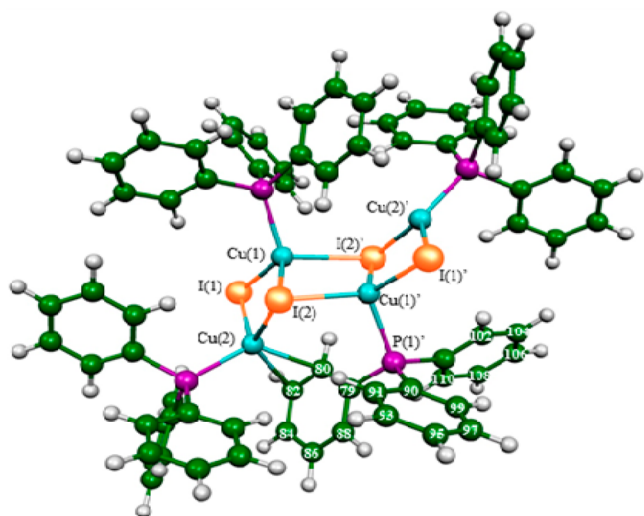

Figure 11. Triplet state (T_2) optimized geometry of **2**.

The nine HOMOs are mainly composed of copper and iodide orbitals with highest contributions of the latter (33% of 3d(Cu) and 58% of 5p(I) orbitals for the HOMO). The 24 LUMOs are closely spaced and largely localized on the phosphine ligands (80−94%) corresponding to combinations of the π^* orbitals of the phenyl groups. Just above this block of LUMOs, there is an orbital (LUMO+24) with a significant 4s/4p(Cu) character (41%) with few iodine admixture (12%) and with still an important π^* contribution (45%). This orbital is significantly Cu−Cu bonding with some Cu−I antibonding character, and its energy is very sensitive to the Cu−Cu distances. The electronic transitions of lowest energy calculated correspond to an electron promotion from the HOMO to one of the lowest π^* combination set (Table 4). Because of the composition of these orbitals, these transitions can be described as ^{1}X,MLCT
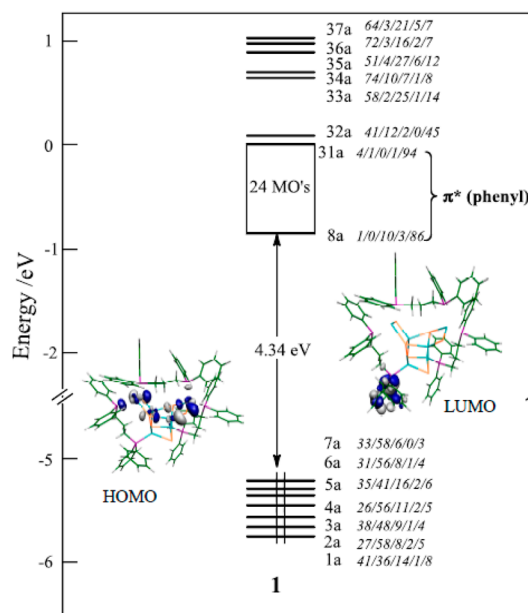

Figure 12. MO diagram of **1** in its ground state. The MO localizations (in %) are given in the following order: Cu/I/P/CH_2/phenyl.

charge-transfer transitions. The absorption spectrum of cluster **1** (Supporting Information, Figure S7) exhibits a broad band centered at 300 nm, which is in agreement with these calculated wavelengths (282−313 nm). The lowest triplet excited state T_1 corresponds to the occupancy of the bonding Cu−Cu (LUMO +24) state so to a combination of different transitions: ^{3}X,MMCT, and ^{3}X,MLCT. The second excited state, T_2, corresponds to the occupancy of the π^* character LUMOs (LUMO − LUMO+23) so to ^{3}X,MLCT transition. These two triplet states are responsible for the two LE and HE emissions observed. The computed emission wavelengths 668 nm (T_1) and 444 nm (T_2) are in rather good agreement with the corresponding experimental values (655 at 290 K and 413 at 77 K in Table 5).

As already mentioned, cluster **1** contains structural features that are present in both **3** ([Cu_4I_4] cubane)) and **2** ([Cu_4I_4] chain), but from the point of view of the lowest excited states the relationship with **3** is straightforward. Whereas the HOMO and the first 24 LUMOs of **1** are of similar nature and composition than those of **3** and **2** (3d(Cu)/5p(I) and π^*(phenyl), respectively), its LUMO+24 resembles that of **3**, that is, is strongly bonding along the six Cu−Cu contacts of the Cu_4 tetrahedron. As in **3**, the optimized T_1 state exhibits short Cu−Cu contacts in the Cu_4 tetrahedron (Table 4). Therefore, by presenting the two T_1 and T_2 excited states, cluster **1** displays thermochromic luminescence properties classically observed for cubane compounds. However, there is one significant difference between clusters **1** and **3** in the nature of the T_1 state. In contrast to **3**, the vacant orbital of Cu−Cu bonding character (LUMO +24) of **1** presents a significant ligand contribution, so this transition comprises a ^{3}X,MLCT character. This can explain the difference in the thermochromism observed for **1**. Indeed, as described previously, **1** displays a concomitant increase of the two bands by lowering the temperature in contrast to the intensities equilibrium observed for **3**. The fact that the LE band intensity still increases upon cooling for **1** can be attributed to decrease of nonradiative phenomena related to the ligand contribution. Actually, this is also the case for **2** with its transition

of ^{3}X,MLCT character whose intensity is very weak at room temperature, which then increases by decreasing the temperature.

Obtaining polymorphs of luminescent species is particularly appealing in establishing structure−property relationships giving straightforward insights into their photophysical properties. In this context, the new cubane cluster **3** reported here deserves discussion in comparison with its related polymorph $[Cu_4I_4(PPh_3)_4]$ (**3P**[16]). At first sight, their luminescence properties are quite similar. Their room-temperature emissions are close: 535 and 545 nm for **3** and **3P**, respectively. They also both display classical luminescence thermochromism by intensities variation of the two LE and HE emission bands. However, when **3** is cooled, the LE band of **3** does not shift in opposite to its polymorph (comparative data in Supporting Information, Figures S8 and S9 and Table S8). From the DFT calculations and previous works,[16,50,51] this red shift is attributed to a change of the Cu−Cu interactions upon cooling. As already mentioned, the LE band (^{3}CC transition) depends on the Cu−Cu bond distances (bonding character); when cooled, these distances decrease, so the excited state lowers its energy and the emission band shifts to longer wavelength. From single-crystal XRD analysis of **3** recorded at different temperatures (300, 250, 200, 150, and 100 K), a shortening of the Cu−Cu bond distances is observed upon cooling (Supporting Information, Table S7). One relevant parameter to account for the global variation of the six Cu−Cu distances in the clusters is the corresponding Cu_4 tetrahedron volume.[25] Thus, by comparing these values with those of the monoclinic polymorph (**3P**),[25] a similar behavior is observed when the sample is cooled with similar rate of shortening for very close values (Supporting Information, Figure S10). This means that in the case of **3**, this shortening is not sufficient to induce changes in the energy of the T_1 state and consequently of the LE emission band. This is quite surprising because the Cu_4 values for both polymorphs are very close. A threshold seems to exist for the Cu−Cu distances to impact the emission energy, and it appears to be exactly around the van der Waals value of 2.80 Å.[47] This agrees with the cubic polymorph presenting even longer Cu−Cu distances and almost no shift.[25] Thus, for **3**, only the relative population of the two excited states (T_1 and T_2) changes with the temperature leading to a perfectly controlled thermochromism with no band shifting.

CONCLUSION

A copper iodide cluster with an original geometry, $[Cu_6I_6(PPh_2$-$(CH_2)_3PPh_2)_3]$ (**1**), which exhibits luminescence thermochromism, has been synthesized. As its molecular structure is based on the $[Cu_6I_6]$ inorganic core derived from the two $[Cu_4I_4]$ chair and cubane isomers, a comparative study has been investigated with $[Cu_4I_4(PPh_3)_4]$ compounds. The luminescence properties observed for these three related copper iodide clusters have been rationalized by DFT calculations giving insights into their different luminescence thermochromism properties.

By exhibiting variation of two emission bands (HE and LE) in temperature, cluster **1** displays thermochromic luminescence properties, which are at first sight similar to those classically observed for copper iodide cubane compound (**3**). This is in accordance with the cubane geometry preserved in the molecular structure of **1**. However, the thermochromism differs by a concomitant increase of the two emission bands by lowering the temperature, in contrast to an equilibrium phenomenon. This can be explained by the different nature of the ^{3}CC transitions, which has in the case of **1**, a significant ligand contribution giving

the corresponding excited state (T_1) a ^{3}X,MLCT character. The nonradiative phenomenon related to the ligand is also responsible for the low intensity of the room-temperature emission of the chair isomer $[Cu_4I_4(PPh_3)_4]$ (**2**). The luminescence properties of the latter are also very different by exhibiting only one single band when cooled. From the DFT calculations, the lack of luminescence thermochromism, opposite to the cubane form, is due to weaker Cu−Cu interactions leading to a second excited state too high in energy to be populated.

A new polymorph of the $[Cu_4I_4(PPh_3)_4]$ cubane cluster has been also characterized (**3**). Compared with its monoclinic polymorph, **3** presents a perfectly controlled thermochromism with no shift of the LE band in temperature. From DFT, the energy of the ^{3}CC state depends on the Cu−Cu interactions, but in the case of **3**, the variation of the Cu−Cu bond distances seems to be insufficient to induce modification of the corresponding emissive state. All these results highlight the sensibility of the emission properties to the cuprophilic interactions. The geometry flexibility of the copper halide compounds allows playing with these interactions giving access to luminophors with an exceptional richness of photophysical properties.

ASSOCIATED CONTENT

S **Supporting Information**

X-ray crystallographic files (CIF), illustrated crystal structures of clusters **1**−**3**, tabulated crystal data and structure refinement parameters for **1**−**3**, experimental and calculated powder XRD diffraction diagrams of clusters **1**−**3**, tabulated experimental and calculated data for clusters **2** and **3**, dielectric constants, NMR spectra of **1**−**3**, emission lifetime curves and corresponding fits for **1** and **3**, MO diagram of **3**, UV−vis spectra of **1**−**3**, DFT data, selected bond lengths and angles. This material is available free of charge via the Internet at http://pubs.acs.org.

AUTHOR INFORMATION

Corresponding Author

*Fax: (+33) (0)1 69 33 47 99. Phone: (+33) (0)1 69 33 46 85. E-mail: sandrine.perruchas@polytechnique.edu.

Notes

The authors declare no competing financial interest.

REFERENCES

(1) Kamtekar, K. T.; Monkman, A. P.; Bryce, M. R. *Adv. Mater.* **2010**, *22*, 572−582.

(2) Fernandez-Moreira, V.; Thorp-Greenwood, F. L.; Coogan, M. P. *Chem. Commun.* **2010**, *46*, 186−202.

(3) Peng, R.; Li, M.; Li, D. *Coord. Chem. Rev.* **2010**, *254*, 1−18.

(4) Wallesch, M.; Volz, D.; Zink, D. M.; Schepers, U.; Nieger, M.; Baumann, T.; Brase, S. *Chem.—Eur. J.* **2014**, *20*, 6578−6590.

(5) Yu, Y.; Zhang, X.-M.; Ma, J.-P.; Liu, Q.-K.; Wang, P.; Dong, Y.-B. *Chem. Commun.* **2014**, *50*, 1444−1446.

(6) Wang, J.-H.; Li, M.; Li, D. *Chem. Sci.* **2013**, *4*, 1793−1801.

(7) Kang, Y.; Wang, F.; Zhang, J.; Bu, X. *J. Am. Chem. Soc.* **2012**, *134*, 17881−17884.

(8) Zink, D. M.; Volz, D.; Baumann, T.; Mydlak, M.; Flügge, H.; Friedrichs, J.; Nieger, M.; Bräse, S. *Chem. Mater.* **2013**, *25*, 4471−4486.

(9) Liu, Z.; Qiu, J.; Wei, F.; Wang, J.; Liu, X.; Helander, M. G.; Rodney, S.; Wang, Z.; Bian, Z.; Lu, Z.; Thompson, M. E.; Huang, C. *Chem. Mater.* **2014**, *26*, 2368−2373.

(10) Perruchas, S.; Le Goff, X. F.; Maron, S.; Maurin, I.; Guillen, F.; Garcia, A.; Gacoin, T.; Boilot, J.-P. *J. Am. Chem. Soc.* **2010**, *132*, 10967−10969.

(11) Shan, X.-C.; Jiang, F.-L.; Chen, L.; Wu, M.-Y.; Pan, J.; Wan, X.-Y.; Hong, M.-C. *J. Mater. Chem. C* **2013**, 4339−4349.

(12) Benito, Q.; Le Goff, X. F.; Maron, S.; Fargues, A.; Garcia, A.; Martineau, C.; Taulelle, F.; Kahlal, S.; Gacoin, T.; Boilot, J.-P.; Perruchas, S. *J. Am. Chem. Soc.* **2014**, *136*, 11311−11320.

(13) Hardt, H. D.; Pierre, A. *Z. Anorg. Allg. Chem.* **1973**, *402*, 107.

(14) Radjaipour, M.; Oelkrug, D. *Ber. Bunsen-Ges.* **1978**, *82*, 159−163.

(15) (a) Ford, P. C.; Cariati, E.; Bourasssa, J. *Chem. Rev.* **1999**, *99*, 3625−3647. (b) Yam, V. W.-W.; Lo, K. K.-W. *Chem. Soc. Rev.* **1999**, *28*, 323−334. (c) Barbieri, A.; Accorsi, G.; Armaroli, N. *Chem. Commun.* **2008**, 2185−2193.

(16) Perruchas, S.; Tard, C.; Le Goff, X. F.; Fargues, A.; Garcia, A.; Kahlal, S.; Saillard, J.-Y.; Gacoin, T.; Boilot, J.-P. *Inorg. Chem.* **2011**, *50*, 10682−10692.

(17) Mézailles, N.; Le Floch, P.; Waschbusch, K.; Ricard, L.; Mathey, F.; Kubiak, C. P. *J. Organomet. Chem.* **1997**, *541*, 277−283.

(18) Liu, Z.; Djurovich, P. I.; Whited, M. T.; Thompson, M. E. *Inorg. Chem.* **2012**, *51*, 230−236.

(19) Naik, S.; Mague, J. T.; Balakrishna, M. S. *Inorg. Chem.* **2014**, *53*, 3864−3873.

(20) Yuan, S.; Liu, S.-S.; Sun, D. *Cryst. Eng. Comm* **2014**, *16*, 1927−1933.

(21) Dyason, J. C.; Healy, P. C.; Engelhardt, L. M.; Pakawatchai, C.; Patrick, V. A.; Raston, C. L.; White, A. H. *J. Chem. Soc., Dalton Trans.* **1985**, 831−838.

(22) Churchill, M. R.; DeBoer, B. G.; Donovan, D. J. *Inorg. Chem.* **1975**, *14* (3), 617−623.

(23) Manbeck, G. F.; Brennessel, W. W.; Evans, C. M.; Eisenberg, R. *Inorg. Chem.* **2010**, *49*, 2834−2843.

(24) Cho, S.; Jeon, Y.; Lee, S.; Kim, J.; Kim, T. H. *Chem.—Eur. J.* **2015**, *21*, 1439−1443.

(25) Kitagawa, H.; Ozawa, Y.; Toriumi, K. *Chem. Commun.* **2010**, *46*, 6302−6304.

(26) Henline, K. M.; Wang, C.; Pike, R. D. *Cryst. Growth Des.* **2014**, *14*, 1449−1458.

(27) Maini, L.; Braga, D.; Mazzeo, P. P.; Ventura, B. *Dalton Trans.* **2012**, *41*, 531−539.

(28) Kupce, E.; Freeman, R. *J. Magn. Reson. Ser. A* **1995**, *115*, 273.

(29) (a) Meiboom, S.; Gill, D. *Rev. Sci. Instrum.* **1958**, *29*, 688. (b) Carr, H. Y.; M. Purcell, E. *Phys. Rev.* **1954**, *94*, 630.

(30) O'Dell, L. A.; Schurko, R. W. *Chem. Phys. Lett.* **2008**, *464*, 97.

(31) Fung, B. M.; Khitrin, A. K.; Ermolaev, K. *J. Magn. Reson.* **2000**, *142*, 97−101.

(32) Cory, D. G.; Ritchey, W. M. *J. Magn. Reson.* **1988**, *80*, 128−132.

(33) Altomare, A.; Burla, M. C.; Camalli, M.; Cascarano, G.; Giacovazzo, C.; Guagliardi, A.; Moliterni, A. G. G.; Polidori, G.; Spagna, R. *SIR97, an integrated package of computer programs for the solution and refinement of crystal structures using single crystal data;* IST, 1999.

(34) Sheldrick, G. M. *SHELXL-97;* Universität Göttingen: Göttingen, Germany, 1997.

(35) Frisch, M. J.; Trucks, G. W.; Schlegel, H. B.; Scuseria, G. E.; Robb, M. A.; Cheeseman, J. R.; Scalmani, G.; Barone, V.; Mennucci, B.; Petersson, G. A.; Nakatsuji, H.; Caricato, M.; Li, X.; Hratchian, H. P.; Izmaylov, A. F.; Bloino, J.; Zheng, G.; Sonnenberg, J. L.; Hada, M.; Ehara, M.; Toyota, K.; Fukuda, R.; Hasegawa, J.; Ishida, M.; Nakajima, T.; Honda, Y.; Kitao, O.; Nakai, H.; Vreven, T.; Montgomery, J. A., Jr.; Peralta, J. E.; Ogliaro, F.; Bearpark, M.; Heyd, J. J.; Brothers, E.; Kudin, K. N.; Staroverov, V. N.; Kobayashi, R.; Normand, J.; Raghavachari, K.; Rendell, A.; Burant, J. C.; Iyengar, S. S.; Tomasi, J.; Cossi, M.; Rega, N.; Millam, N. J.; Klene, M.; Knox, J. E.; Cross, J. B.; Bakken, V.; Adamo, C.; Jaramillo, J.; Gomperts, R.; Stratmann, R. E.; Yazyev, O.; Austin, A. J.; Cammi, R.; Pomelli, C.; Ochterski, J. W.; Martin, R. L.; Morokuma, K.; Zakrzewski, V. G.; Voth, G. A.; Salvador, P.; Dannenberg, J.J.; Dapprich, S.; Daniels, A. D.; Farkas, Ö.; Foresman, J. B.; Ortiz, J. V.; Cioslowski, J.; Fox, D. J. *Gaussian 09,* Revision D.01; Gaussian, Inc.: Wallingford, CT, 2009.

(36) (a) Perdew, J. P.; Ernzerhof; Burke, K. M. *J. Chem. Phys.* **1996**, *105*, 9982. (b) Perdew, J. P.; Burke, K.; Ernzerhof, M. *Phys. Rev. Lett.* **1996**, *77*, 3865. (c) Perdew, J. P.; Burke, K.; Ernzerhof, M. *Phys. Rev. Lett.* **1997**, *78*, 1396.

(37) (a) Dunning Jr., T. H.; Hay, P. J.; *Methods of Electronic Structure Theory;* Schaeffer, H. F. ed., Plenum Press: New York, 1977. (b) Hay, P. J.; Wadt, W. R. *J. Chem. Phys.* **1985**, *82*, 270. (c) Hay, P. J.; Wadt, W. R. *J. Chem. Phys.* **1985**, *82*, 284. (d) Hay, P. J.; Wadt, W. R. *J. Chem. Phys.* **1985**, *82*, 299.

(38) Scalmani, G.; Frisch, M. J. *J. Chem. Phys.* **2010**, *132*, 114110−144124.

(39) Gorelsky, S. I. AOMix program. http://www.sg-chem.net.

(40) Burke, K.; Gross, E. K. U. A Guided Tour of Time-Dependent Density Functional Theory. In *Density Functionals: Theory and Applications, Lecture Notes in Physics;* Joubert, D., Ed.; Springer: New York, 1998; Vol. *500*.

(41) Flukiger, P.; Luthi, H. P.; Portmann, S.; Weber, J. *MOLEKEL 4.3;* Swiss Center for Scientific Computing: Manno, Switzerland, 2000. http://www.cscs.ch/.

(42) (a) London, F. *J. Phys. Radium* **1937**, *8*, 397−409. (b) McWeeny, R. *Phys. Rev.* **1962**, *126*, 1028−1034. (c) Ditchfield, R. *Mol. Phys.* **1974**, *27*, 789−807. (d) Dodds, J. L.; McWeeny, R.; Sadlej, A. *J. Mol. Phys.* **1977**, *34*, 1779−1791. (e) Wolinski, K.; Hinton, J. F.; Pulay, P. *J. Am. Chem. Soc.* **1990**, *112*, 8251−8260. (f) Cheeseman, J. R.; Trucks, G. W.; Keith, T. A.; Frisch, M. J. *J. Chem. Phys.* **1996**, *104*, 5497−509.

(43) Weigend, F.; Ahlrichs, R. *Phys. Chem. Chem. Phys.* **2005**, *7*, 3297−3305.

(44) Adiga, S.; Aebi, D.; Bryce, D. L. *Can. J. Chem.* **2007**, *85*, 496−505.

(45) Massiot, D.; Fayon, F.; Capron, M.; King, I.; Le Calvé, S.; Alonso, B.; Durand, J. O.; Bujoli, B.; Gan, Z.; Hoatson, G. *Magn. Reson. Chem.* **2002**, *40*, 70−76.

(46) Arkhireeva, T. M.; Bulychev, B. M.; Sizov, A. I.; Sokolova, T. A.; Belsky, V. K.; Soloveichik, G. L. *Inorg. Chim. Acta* **1990**, *169*, 109.

(47) Bondi, A. *J. Phys. Chem.* **1964**, *68*, 441.

(48) (a) Fackler, J. P. *Inorg. Chim. Acta* **2015**, *424*, 83. (b) Dinda, S.; Samuelson, A. G. *Chem.—Eur. J.* **2012**, *18* (10), 3032. (c) Sculfort, S.; Braunstein, P. *Chem. Soc. Rev.* **2011**, *40*, 2741. (d) Gao, G.-F.; Li, M.; Zhan, S.-Z.; Lv, Z.; Chen, G.; Li, D. *Chem.—Eur. J.* **2011**, *17*, 4113.

(49) Tang, J. A.; Ellis, B. D.; Warren, T. H.; Hanna, J. V.; Macdonald, C. L. B.; Schurko, R. W. *J. Am. Chem. Soc.* **2007**, *129*, 13049−13065.

(50) Kim, T. H.; Shin, Y. W.; Jung, J. H.; Kim, J. S.; Kim, J. *Angew. Chem., Int. Ed.* **2008**, *47*, 685−688.

(51) Sun, D.; Yuan, S.; Wang, H.; Lu, H.-F.; Feng, S.-Y.; Sun, D.-F. *Chem. Commun.* **2013**, *49*, 6152−6154.